

Nucleosynthesis of Nickel-56 from Gamma-Ray Burst Accretion Disks

R. Surman¹, G. C. McLaughlin², and N. Sabbatino¹

ABSTRACT

We examine the prospects for producing Nickel-56 from black hole accretion disks, by examining a range of steady state disk models. We focus on relatively slowly accreting disks in the range of $\dot{M} = 0.05 M_{\odot}/s$ to $\dot{M} = 1 M_{\odot}/s$, as are thought to be appropriate for the central engines of long-duration gamma-ray bursts. We find that significant amounts of Nickel-56 are produced over a wide range of parameter space. We discuss the influence of entropy, outflow timescale and initial disk position on mass fraction of Nickel-56 which is produced. We keep careful track of the weak interactions to ensure reliable calculations of the electron fraction, and discuss the role of the neutrinos.

Subject headings: gamma ray:bursts-nucleosynthesis-accretion disks

1. Introduction

Over the last decade and a half there has been a dramatic increase in data available for studying long duration gamma-ray bursts (GRBs). Besides the gamma rays, afterglows in the x-ray, optical and radio are seen, and host galaxies have been identified. In a handful of cases “supernova bumps” are seen in the optical afterglows, e.g. GRB 980326 (Bloom et al. 1999). Furthermore, spectra for Type Ic supernova have been identified in a few cases (Galama et al. 1998; Hjorth et al. 2003; Kawabata et al. 2003; Matheson et al. 2003; Stanek et al. 2003; Malesani et al. 2004; Thomsen et al. 2004). These developments have lead to the theoretical conjecture that all long duration gamma ray bursts are the result of the collapse of a massive star; for a review see Woosley & Bloom (2006).

The temporal evolution of light curve spectra of traditional core collapse supernovae are driven by the decay of Nickel-56 to Cobalt-56 and the subsequent decay of Cobalt-56 to Iron-56. The half lives for these decays are approximately six days and

seventy-seven days respectively. After these nuclei beta decay, their daughter nuclei emit gamma rays which then thermalize in the ejecta. The energy from these decays is thus re-emitted in the optical and observed as the supernova light curve. Thus the intensity of a supernova bump should be directly influenced by the amount of ^{56}Ni produced in the object. On the order of tenths of solar masses of Nickel are needed. For example, it has been estimated that around $0.5M_{\odot}$ of ^{56}Ni is necessary to explain SN2003dh which accompanied GRB030329 (Woosley and Heger 2003).

The commonly discussed model for the type of supernova that produces a GRB is the collapsar model (Woosley 1993; MacFadyen & Woosley 1999). In this case the star has too much rotation to produce a standard core collapse supernova. A hot ~ 10 MeV disk surrounding a black hole is produced at the center. Nickel-56 can be produced in two different ways. It can be produced in explosive burning, when a shock wave propagates out through the star and pre-existing nuclei are then burned to ^{56}Ni (Maeda & Nomoto 2003; Fryer et al. 2006; Maeda & Tominaga 2009). This is the same mechanism as in traditional core collapse supernovae, but the elemental yields are different since the explosion energy is larger. However, Nickel-56 can also be produced in a disk

¹Department of Physics and Astronomy, Union College, Schenectady, NY 12308

²Department of Physics, North Carolina State University, Raleigh, NC 27695-8202

wind. This is a primary process where free neutrons and protons are ejected from the disk and combine to form nuclei (Surman & McLaughlin 2005; Pruet, Thompson, & Hoffman 2004; Surman et al. 2006).

Any assessment of ^{56}Ni production in GRBs must consider both mechanisms. The latter mechanism is more difficult to model, since it requires a careful accounting of the neutrinos in the disk. In this paper we extend the preliminary studies of Surman & McLaughlin (2005); Pruet, Thompson, & Hoffman (2004); Pruet, Surman, & McLaughlin (2005); Surman et al. (2006), and examine the production of Nickel-56 from the outflow from a variety of disks. We discuss not only the importance of the electron fraction in determining the abundance yields, but also the role of entropy and outflow timescale. Recent studies, e.g. Maeda & Tominaga (2009) and references therein, have used estimates of ejected ^{56}Ni mass to constrain the GRB central engine. This study provides a reference for anyone considering Nickel-56 production in models of long duration gamma-ray bursts.

2. Disk and Outflow models

In order to study the nucleosynthesis in the hot outflows from GRB accretion disks, we first need to determine the composition of and the neutrino fluxes emitted from the accretion disk itself. We therefore begin with existing hydrodynamical black hole accretion disk (AD-BH) models with parameters appropriate for long-duration GRBs. For this study we have chosen the one-dimensional, steady-state AD-BH models of Chen & Beloborodov (2007) (CB). The CB models are fully relativistic and incorporate important microphysics effects, such as neutrino trapping and an evolving neutron-to-proton ratio, neglected in other relativistic disk calculations. Here we investigate a range of steady-state disk models with mass accretion rates $0.05 \leq \dot{m} \leq 1$, where $\dot{m} = 1 M_{\odot}/\text{s}$.

We calculate the initial nuclear composition of each disk as described in Surman & McLaughlin (2004). We find the disk compositions we calculate as a post-processing step match well with the disk compositions reported in Chen & Beloborodov (2007), which are calculated along with the disk

hydrodynamics. In the inner regions of all of the disks, nuclei are dissociated into their constituent nucleons, and the ratio of neutrons to protons is subsequently set by the weak interactions

$$p + e^{-} \rightleftharpoons n + \nu_e \quad (1)$$

$$n + e^{+} \rightleftharpoons p + \bar{\nu}_e. \quad (2)$$

We describe the composition of the disks by the electron fraction Y_e , where $Y_e = 1/(1 + n/p)$ and n and p are the number densities of neutrons and protons, respectively. For disks with the lowest accretion rates of those considered here, weak reaction rates are slow even in the inner regions of the disks. In these cases the disk composition remains roughly balanced between neutrons and protons and Y_e remains close to 0.5. For disks with higher accretion rates, conditions in the inner region of the disks are hotter and denser, and weak reactions are correspondingly faster. For disks with $\dot{m} < 1$, electron capture on protons, the forward reaction of Eqn. 1, predominates, and the inner regions of the disks become quite neutron rich. Fig. 1 shows the electron fractions in the disk for two radial distances, $r_0 = 50$ km and 100 km, from the black hole for the disk models used in this work. A full discussion of the disk compositions of AD-BH can be found in, for example, Pruet, Woosley, & Hoffman (2003); Fujimoto et al. (2003); Surman & McLaughlin (2004); Chen & Beloborodov (2007). These disk electron fractions provide the starting points for the calculations of the nucleosynthesis from the disks.

While calculating the composition of the disks, we additionally calculate the neutrino fluxes from the disk as in Surman & McLaughlin (2004). Most of the AD-BHs considered in this work are optically thin to neutrinos and the emitted fluxes are primarily due to electron and positron captures in the disk. Since the rate of electron captures in the disks far exceeds the rate of positron captures for all disks with $\dot{m} \geq 0.1$, the electron neutrino flux emitted from the disk is significantly higher than the electron antineutrino flux. This has important consequences for the nucleosynthesis in the outflow.

We follow the outflowing material as described in Surman & McLaughlin (2005). We take the outflow to be adiabatic and the velocity v of the outflowing material as a function of radial distance

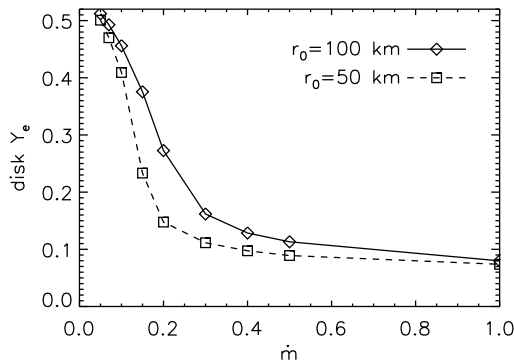


Fig. 1.— Shows the electron fractions in the disk at radial distances of $r_0 = 50$ km (squares) and $r_0 = 100$ km (diamonds) for AD-BH with mass accretion rates \dot{m} .

from the black hole r to be $v = v_\infty(1 - r_0/r)^\beta$, with $v_\infty = 10,000$ km/s, r_0 is the starting disk position, and β controls the rate of the acceleration of the material. We investigate a range of β , $0.2 \leq \beta \leq 2.6$, where smaller β corresponds to more rapid initial acceleration, and two disk starting positions, $r_0 = 50$ km and 100 km. We connect the evolution of the density to our velocity prescription by setting the mass loss rate \dot{M} of the outflow to be constant, first in cylindrical symmetry as the material lifts off vertically from the disk, and then in spherical symmetry as the material expands radially away at later times. We take the initial composition of the material to be that of the disk at the starting radius r_0 . We then follow the nuclear recombination using a full nuclear network code as described in Surman et al. (2006). A schematic of the outflow is shown in Fig. 2.

While the entropy of the disk is quite low, several potential heating processes can increase the entropy of the material as it lifts off the disk. To make some estimate of what range in entropies is realistic for the wind, we consider the rate of change of entropy due to just one potential heating source—neutrino captures in the outflow. We start with the approximate expressions for the neutrino heating and cooling rates from Qian & Woosley (1996) and calculate the change in entropy per baryon from energy conservation, recast for a neutrino-driven wind in Eqn (26) of

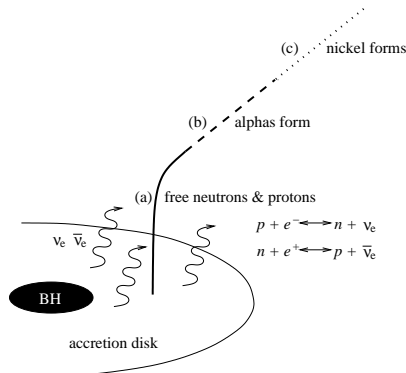


Fig. 2.— Shows a schematic of an outflow trajectory, labeled with the three stages of outflow nucleosynthesis.

Qian & Woosley (1996) as

$$v \frac{ds}{dr} = \frac{\dot{q} m_N}{T}, \quad (3)$$

where s is the entropy per baryon, m_N is the mass of a nucleon, T is the temperature, and \dot{q} is the specific net heating rate due to neutrino and antineutrino interactions. When we apply this expression to our outflow velocity and density profiles as described above, we find, for example, for an $\dot{m} = 0.15$ disk, the change in entropy per baryon in the outflow due to neutrino interactions ranges from $1 - 23k$, while for a $\dot{m} = 1$ disk, the range is $4 - 58k$. We note that these estimates represent a lower limit, as additional processes (e.g., magnetic heating) are expected to play an important role. We therefore investigate outflow entropies up to somewhat larger values, $10 \leq s/k \leq 100$.

3. Production of Nickel-56

The element synthesis leading to the production of ^{56}Ni for a sample AD-BH outflow trajectory is depicted in Fig. 3, which shows the evolution of the mass fractions of neutrons, protons, alpha particles, and ^{56}Ni as a function of decreasing temperature T_9 , where $T_9 = T/10^9$ K and T is the temperature in the outflow in Kelvins. In this example, the material is ejected from an AD-BH with $\dot{m} = 0.5$ at a starting radius of $r_0 = 100$ km; the initial composition is therefore quite neutron rich. As the material lifts off the disk, it transitions from the dense, low entropy, electron-degenerate

disk conditions to the higher entropy ($s/k = 30$ in this example), hotter, accelerated outflow conditions. The higher entropy favors a balance of electrons and positrons such that positron capture, the forward reaction of Eqn. 2, can compete with electron capture, and the electron fraction quickly rises. As the material moves away from the disk, it cools and expands, and weak reaction rates slow. Even so, the electron fraction continues to evolve as the positron capture rate, and eventually the electron neutrino capture (the reverse reaction of Eqn. 1) rate, are slightly faster than the electron capture rate. The positron capture rate exceeds the electron capture rate because of the neutron-proton mass difference, and eventually the electron neutrino capture rate exceeds both the electron and positron capture rates as the latter drop much more rapidly ($\sim T^{-5}$) above the disk. Therefore the material gradually becomes proton-rich prior to nuclear reassembly, as seen in Fig. 3 for $T_9 > 10$. This portion of the outflow trajectory, where the material is composed of free nucleons and their ratio is adjusted by weak interactions, is labeled (a) in Figs. 2 and 3.

In the first stage of nuclear reassembly, labeled (b) in Figs. 2 and 3, protons and neutrons combine into alpha particles (^4He nuclei). Conversion into alphas is most efficient at $Y_e = 0.5$, where equal numbers of protons and neutrons are present. In this example, the material is slightly proton-rich, so all of the neutrons and a matching number of protons combine into alphas, and a small fraction of excess protons are left over. In the second stage of nuclear reassembly, labeled (c) in Figs. 2 and 3, alpha particles combine via the triple alpha process to produce ^{12}C , and a series of alpha captures on carbon culminate in the production of ^{56}Ni . The triple-alpha process and the subsequent alpha captures are highly temperature-dependent, and so the efficiency of the conversion of alphas to ^{56}Ni depends strongly on the evolution of the thermodynamic conditions in the outflow. If the outflow is coasting at this point such that the temperature drops slowly, most of the alphas will convert to nickel; in the example considered here, however, this isn't quite the case, and a bit more than one half of the alphas end up in ^{56}Ni .

The production of ^{56}Ni can therefore depend on a number of parameters: the mass accretion rate of the AD-BH, the point in the AD-BH at which

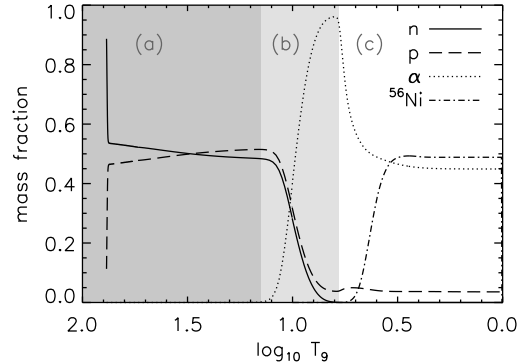


Fig. 3.— Shows the mass fractions of neutrons (solid line), protons (dashed line), alphas (dotted line) and ^{56}Ni (dot-dashed line) as a function of decreasing temperature T_9 for an outflow trajectory with parameters $r_0 = 100$ km, $s/k = 30$, and $\beta = 0.8$ from an AD-BH with $\dot{m} = 0.5$. The shaded areas refer to the portions of the outflow trajectory where (a) the ratio of free protons to neutrons is set by weak interactions (dark shaded region), (b) protons and neutrons combine to form alphas (light shaded region), and (c) alphas combine to make ^{56}Ni (unshaded region).

the outflow originates, the entropy per baryon and the acceleration of the outflow, and the neutrino interactions in the outflow. The influence of each of these parameters in turn is described in sections 3.1-3.3 below.

3.1. Variation with entropy

The production of nickel depends sensitively on the entropy per baryon in the outflowing material. Fig. 4 shows the final mass fraction of ^{56}Ni in the disk outflow as a function of the mass accretion rate \dot{m} of the AD-BH and the entropy s/k in the outflow, for a sample set of trajectories with starting disk position $r_0 = 100$ km and wind parameter $\beta = 0.2$. We see vigorous production of ^{56}Ni over the majority of the parameter space. Interestingly, for $\dot{m} \geq 0.2$, the production of nickel does not appear to depend strongly on the accretion rate of the AD-BH and is instead a much stronger function of the entropy per baryon in the outflow.

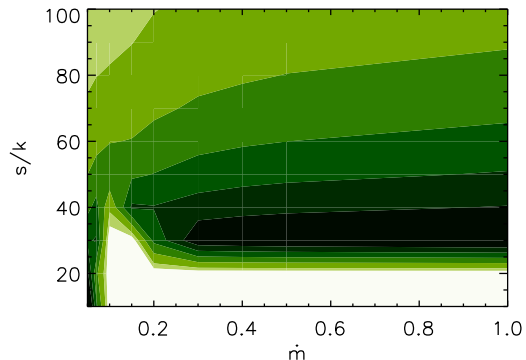


Fig. 4.— Shows nickel production as a function of the entropy s/k of the outflowing material and the mass accretion rate \dot{m} of the disk from which the material originates. All trajectories shown have a starting disk position of $r_0 = 100$ km and wind parameter $\beta = 0.2$, which corresponds to rapid initial acceleration. The shaded regions indicate mass fractions of ^{56}Ni in excess of 0.5 (darkest shaded region), 0.4, 0.3, 0.2, 0.1, 0.05, and less than 0.05 (unshaded region).

3.1.1. $\dot{m} \geq 0.2$

First we consider the nickel production in outflows from the AD-BHs with $\dot{m} \geq 0.2$. In the outflow trajectories with $s/k \leq 20$, the entropy is not much higher than in the disk itself and so the material retains some of the neutron richness of the disk. In these cases, the neutron excess remaining after alpha-particle assembly leads to neutron captures on the alpha-capture chain nuclei, and heavier isotopes of nickel predominate. Outflow trajectories with $s/k > 20$ are sufficiently high in entropy such that the neutron richness of the disk is erased by positron capture in the outflow. The most efficient production of ^{56}Ni occurs just at this transition between neutron-rich and proton-rich, where $Y_e = 0.5$; for the trajectories considered in Fig. 4 this occurs when $s/k \sim 30$. At even higher entropies, the assembly into alphas is shifted to later times, and the weak reactions on free nucleons have more time to drive the material proton rich. Therefore as we consider outflow trajectories with various entropies, we find the higher entropy cases produce higher Y_e and thus less efficient production of ^{56}Ni .

3.1.2. $\dot{m} < 0.2$

The outflows from AD-BHs with $\dot{m} < 0.2$ differ slightly from the above picture. Disks with lower mass accretion rates have lower central disk temperatures and densities. The most important effect of this for disks with $0.1 \leq \dot{m} < 0.2$ is that the outflows have lower starting temperatures and densities. This means the weak rates are not necessarily fast enough for the electron fraction to reequilibrate in the outflow prior to nuclear reassembly, and so the neutron richness of the disk is retained to higher entropies. For the lowest mass accretion rate disks considered in this work, $0.05 \leq \dot{m} < 0.1$, the central disk temperatures and densities are sufficiently low that the composition of the disk remains fairly balanced between neutrons and protons, as shown in Fig. 1. The outflows from these disks therefore have electron fractions close to a half—and correspondingly strong ^{56}Ni production—at lower entropies.

3.2. Variation with β

While the entropy per baryon in the outflow plays a central role in setting the electron fraction, another important ingredient is the time available for each stage of the nucleosynthesis. In our outflow parameterization this is set by the wind parameter β , which determines the initial acceleration of the outflow material. Fig. 5, similarly to Fig. 4, shows the final mass fraction of nickel in the outflowing material as a function of the mass accretion rate \dot{m} of the AD-BH and the entropy s/k in the outflow, for a sample set of trajectories with starting disk position $r_0 = 100$ km and wind parameters $\beta = 0.8, 1.4, 2.0$, and 2.6 . As shown in Fig. 5, increases in β decrease the overall efficiency of ^{56}Ni production and, for high values of β , shift the entropy per baryon s/k of the most efficient production.

In order to understand the decrease in efficiency with increasing β , consider that the most robust ^{56}Ni production occurs when the outflow conditions evolve (1) sufficiently rapidly at early times to prevent the material from becoming too proton-rich and (2) sufficiently slowly at late times to facilitate the complete conversion of alphas to ^{56}Ni . Small values of β correspond to rapid initial acceleration where the material quickly attains coasting speed, while outflows with large values of β

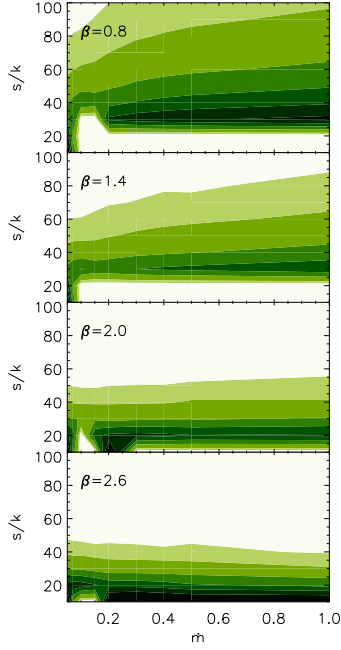


Fig. 5.— Similar to Fig. 4, but for wind parameters $\beta = 0.8, 1.4, 2.0$, and 2.6 .

accelerate slowly at first and evolve more rapidly at later times. This effect is illustrated in Table 1, which shows the average values of the outflow velocity \dot{r} divided by the radial distance of the material r for two key points in the evolution of the outflow—at early times when the electron fraction is set by weak interactions and late times during nuclear reassembly. The value of \dot{r}/r serves as an indicator of how rapidly conditions evolve during these key periods; robust ^{56}Ni production therefore requires large values of \dot{r}/r at early times and small values at late times. As Table 1 shows, these conditions are satisfied in trajectories with the smallest values of β . Trajectories with larger β evolve too rapidly at late times to efficiently synthesize nickel, and, as shown in the table, most of the material is left as alpha particles.

For very high β , $\beta \geq 2.0$, the most efficient ^{56}Ni production shifts to lower entropies. This effect is due to the influence of neutrino interactions in the outflow. As shown in Table 1, the evolution of the outflow for high β is slow at early times, when

the material is close to the disk. The high β trajectories, therefore, receive the highest neutrino fluence. Since the electron neutrino flux from the disk is significantly higher than the electron antineutrino flux, the net influence of the neutrinos is to drive the material proton rich via the reverse reaction in Eqn. 1. The low entropy trajectories that, in the absence of the neutrino interactions, would be neutron rich become proton rich and can therefore effectively produce ^{56}Ni , as illustrated in Fig. 6.

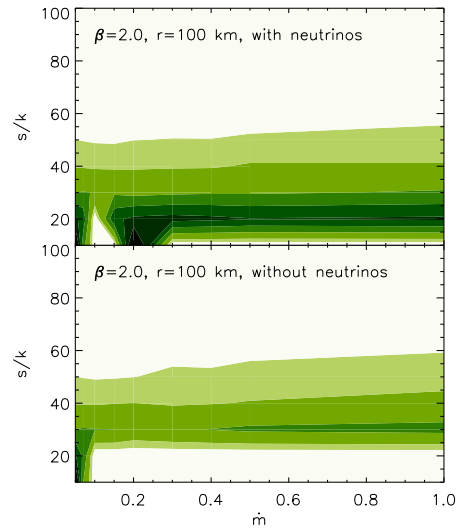


Fig. 6.— The top panel is identical to the third panel of Fig. 5, which shows nickel production as in Fig. 4 for wind parameters $\beta = 2.0$ and $r_0 = 100$ km. The bottom panel is identical except the neutrino interactions in the outflow have been turned off.

3.3. Variation with starting disk position

While the outflow nucleosynthesis is primarily dependent on the outflow conditions as described above, the initial conditions—the local disk conditions at the point of origin of the outflow—also have some bearing on the final nickel production. Fig. 7, similarly to Fig. 4, shows the mass fraction of nickel in the outflowing material as a function of the mass accretion rate \dot{m} of the AD-BH and the entropy s/k in the outflow, for a sample set of trajectories with $\beta = 1.4$ and two starting disk

positions, $r_0 = 50$ km and 100 km. Nickel production is similar in both cases, though trajectories originating from the inner disk region are somewhat less efficient. This is due to two separate effects—the influence of neutrino interactions and the starting temperature of the material. In the disk itself, the temperatures and densities increase with decreasing radius, and correspondingly the rates of weak reactions, and therefore the emission of neutrinos, also increase. Thus the material outflowing from smaller radii will have higher initial temperatures and densities than outflows from larger disk radii, and the neutrino flux the material is exposed to in the outflow will be higher. The latter effect tends to increase the electron fraction of the material; for trajectories that are already proton rich this decreases the efficiency of alpha particle formation. The former effect—the larger of the two—postpones alpha particle reassembly to later times and farther distances in the outflow. As shown in Table 1, the velocity divided by radial distance \dot{r}/r is faster during the epoch of alpha particle reassembly for smaller starting radii, resulting in less efficient nickel production.

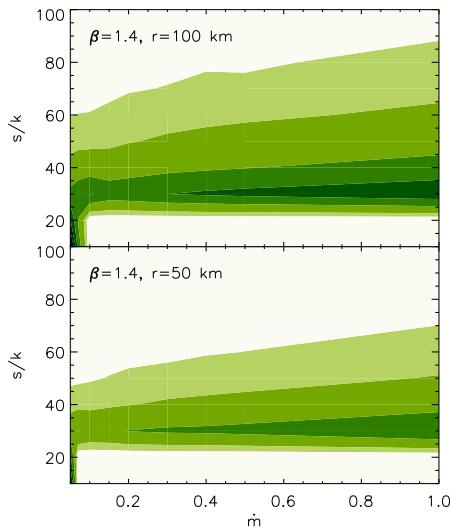


Fig. 7.— Similar to Fig. 4, but for wind parameter $\beta = 1.4$ and starting disk positions $r_0 = 100$ km and 50 km.

4. Additional nucleosynthesis

While in this work our focus is on the production of Nickel-56, we note that other interesting nuclear species may also be synthesized in the outflow. Trajectories with strong Nickel-56 production can make a number of intermediate mass nuclei that are underproduced in galactic chemical evolution studies, such as ^{45}Sc , ^{49}Ti , and ^{64}Zn (Pruet, Surman, & McLaughlin 2005). Low entropy ($s/k \leq 20$) trajectories from disks with $\dot{m} > 0.1$ are moderately neutron rich; these outflows produce heavier nickel isotopes and $N = 50$ nuclei, and can potentially make some light r -process nuclei. High entropy ($s/k \geq 50$) trajectories with slow initial acceleration can make some interesting light p -process nuclei such as ^{74}Se , ^{78}Kr , ^{84}Sr , and ^{92}Mo .

An example of the latter two types of nucleosynthesis is shown in Fig. 8, which compares the final mass fraction of the light p -nucleus ^{92}Mo produced in the outflow to its solar mass fraction. The origin of this nucleus has long been a mystery, though studies of the newly-discovered νp process (Frohlich et al. 2006; Pruet et al. 2006) suggest early supernova neutrino-driven winds to be a strong candidate site for its production. Here we examine its production in the context of our GRB outflow models.

In the case of the moderately accelerating outflow, $\beta = 1.4$, we see strong ^{92}Mo production for low entropies, where the material is moderately neutron-rich. However, here the synthesis of ^{92}Mo is accompanied by excessive overproduction of some $N = 50$ closed shell nuclei such as ^{88}Sr , ^{89}Y , and ^{90}Zr . The overproduction of $N = 50$ nuclei is so large (greater than a factor of 10^5 over solar in some cases) for these trajectories that if one knew precisely the amount of disk outflow and the rate at which accretion disks are formed, one could in principle constrain the disk wind conditions from this information.

Alternately, we see that for the case of the outflows with slow initial acceleration, $\beta = 2.6$, the greatest ^{92}Mo production occurs at high entropies, from disks with the most vigorous neutrino emission. These trajectories have electron fractions greater than 0.6 and experience the highest neutrino fluence, both requirements for a successful νp process. The production of ^{92}Mo and other light

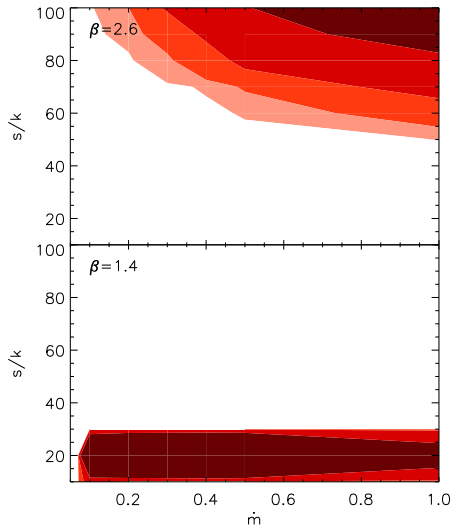


Fig. 8.— Shows the final mass fraction of light p -process nucleus ^{92}Mo divided by its solar value, for wind parameters $\beta = 1.4$ (bottom panel) and $\beta = 2.6$ (top panel), and $r_0 = 100$ km. The shaded regions indicate ^{92}Mo production ratios in excess of 10000 (darkest shaded region), 1000, 100, and 10 (lightest shaded region).

p nuclei via a νp process in GRB disk outflows has been discussed in Kizivat et al. (2010).

5. Alternate outflow model

Finally, for comparison we consider an alternate, spherical outflow model in which the evolution of the electron fraction is tied more closely to the hydrodynamics. We construct the model by first constraining the outflow to follow radial streamlines with zero vorticity. This, along with the steady flow approximation, implies the Bernoulli function is constant along the streamline that defines the outflow trajectory. In its simplest form, the Bernoulli function is

$$B = \frac{1}{2}v^2 + h + \Phi, \quad (4)$$

where v is the velocity, h is the specific enthalpy, and Φ is the gravitational potential due to the black hole, $-GM_{\text{BH}}/r$. We write the specific en-

thalpy as

$$h = \frac{1}{\rho} \left[\sum_i n_i \mu_i + (kT)(s/k)n_B \right], \quad (5)$$

where n_B is the baryon number density, and n_i and μ_i are the number density and chemical potential, respectively, of species i , where the sum over species includes electrons, positrons, neutrons, protons, alpha particles, and an average heavy nucleus. We solve for the outflow hydrodynamics by further assuming adiabatic flow and a constant mass outflow rate, $\dot{M} = 4\pi r^2 \rho v$. We evolve the composition of the outflowing material as described in Sec. 2.

The spherical outflow model differs from the parameterized wind primarily in the shape of the outflow trajectory—which is purely radial with no initial vertical piece—and the significantly slower acceleration of the outflowing material. Both of these effects impact the extent to which neutrino interactions influence the resulting nucleosynthesis, though in opposite directions. A purely radial trajectory moves material away from the central disk region, which is the source of the hottest neutrinos, more directly than initially-vertical flow. However, this effect is dwarfed here by the effect of the dramatically larger neutrino fluence that arises due to the slower acceleration. The initial flow is so much slower that the electron fraction re-equilibrates in the outflow in every case, to values above 0.5. For the low mass accretion rate disks, this results in vigorous ^{56}Ni production, as shown in Fig. 9. However, in higher accretion rate disks that have non-negligible antineutrino emission, the production of nickel shifts to heavier isotopes. This is due to a mini- νp -like process, whereby antineutrino interactions on the free protons remaining after the onset of heavy element formation create neutrons that are quickly captured by nuclei, primarily the dominant ^{56}Ni . The result is a shift from ^{56}Ni to ^{58}Ni and finally to ^{60}Ni with increasing disk \dot{m} , as shown in Fig. 9, compared to the almost constant production of ^{56}Ni that results when neutrino interactions are neglected.

6. Conclusion

Nickel production in the outflows from black hole accretion disks may be an important com-

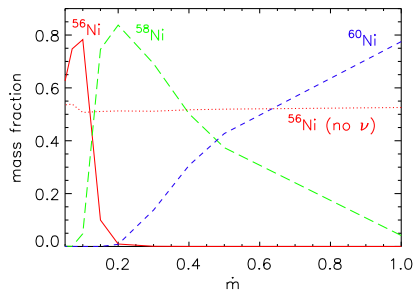


Fig. 9.— Shows the final mass fractions of ^{56}Ni (solid red line), ^{58}Ni (long-dashed green line), and ^{60}Ni (short-dashed blue line) as a function of disk mass accretion rate \dot{m} , for the spherical outflow model with $s/k = 40$ and $r_0 = 50$ km, compared to the final mass fraction of ^{56}Ni (dotted red line) obtained with the same outflow model but without neutrino interactions.

ponent of the total GRB Nickel-56 production. We have outlined the ways in which ^{56}Ni can be formed by black hole accretion disks under a variety of conditions, taking careful account of the neutrino interactions.

We find that entropy is a strong diagnostic across a broad range of accretion disk models. Nickel production appears to be optimal for only modest increases in entropy over the in-disk values; for the disks studied here with $\dot{m} > 0.1$, this can be accounted for via neutrino heating alone. We note that nickel can also be produced via thermonuclear burning from a shock that goes through a star, if the disk is associated with a hypernova explosion. However, in models without this additional production mechanism, one could constrain the required conditions for nickel production in the object. For example, if accretion disk outflows are to be a significant fraction of the overall GRB nickel production, the contribution of other processes, such as magnetic heating, to the entropy increase in the outflow from $\dot{m} > 0.1$ disks should not greatly exceed that of the neutrino interactions.

However, conclusions about the mass fraction of Nickel produced cannot be drawn from the entropy alone. Nickel formation is optimized when the outflow timescale, in particular the ratio of \dot{r}/r in the outflow, is fast at the beginning stages of nu-

cleosynthesis and slow later. Furthermore, in the models considered here, outflows from an intermediate disk radius, $r_0 \sim 100$ km, more efficiently produced nickel than material ejected closer to the black hole. Under the optimal conditions up to around 50% of the material ejected from black hole accretion disks will become Nickel-56. These results, when coupled with future wind model calculations and observations, can ultimately be used to constrain the outflow conditions of GRB disks.

This work was partially supported by the Department of Energy under contract DE-FG02-02ER41216 (GCM) and under contract DE-FG02-05ER41398 (RS), and the National Science Foundation ADVANCE Grant 0820032 (RS).

REFERENCES

- Bloom, J. S., et al. 1999, *Nature*, 401, 453
- Chen, W.-X. & Beloborodov, A., 2007, *ApJ*, 657, 383
- Frohlich, C. et al. 2006, *ApJ*, 637, 415
- Fryer, C. L., Young, P. A., & Hungerford, A. L. 2006, *ApJ*, 650, 1028
- Fujimoto, S., Hashimoto, M., Koike, Arai, K., & Matsuba, R. 2003 *ApJ*, 585, 418
- Galama, T. J., et al. 1998, *Nature*, 395, 670
- Hjorth, J., et al. 2003, *Nature*, 423, 847
- Kawabata, K. et al. 2003, *ApJ*, 593, L19
- Kizivat, L.-T., Martinez-Pinedo, G., Langanke, K., Surman, R., & McLaughlin, G. C. 2010, *Phys. Rev. C*, 81, 025802
- MacFadyen, A. I. & Woosley, S. E. 1999, *ApJ*, 524, 262
- Maeda, K. & Nomoto, K. 2003, *ApJ*, 598, 1163
- Maeda, K., & Tominaga, N. 2009, *MNRAS*, 288
- Malesani D., et al. 2004, *ApJ*, 609, L5
- Matheson T., et al. 2003, *ApJ*, 599, 394
- Pruet, J., Woosley, S. E., & Hoffman, R. D. 2003, *ApJ*, 586, 1254

Pruet, J., Thompson, T., & Hoffman, R. D. 2004, ApJ, 606, 1006

Pruet, J., Hoffman, R. D., Woosley, S. E., Janka, H.-T., & Buras, R. 2006, ApJ, 644, 1028

Pruet, J., Surman, R., & McLaughlin, G. C. 2005, ApJ, 602, L101

Qian, Y.-Z. & Woosley, S. E. 1996, ApJ, 471, 331

Stanek, K. Z., et al. 2003, ApJ, 591, L17

Surman, R. & McLaughlin, G. C. 2004, ApJ, 603, 611

Surman, R. & McLaughlin, G. C. 2005, ApJ, 618, 397

Surman, R., McLaughlin, G. C., & Hix, W. R. 2006, ApJ, 643, 1057

Thomsen B., et al. 2004, A&A, 419, L21

Woosley, S. E. 1993, ApJ, 405, 273

Woosley S.E., Bloom J.S. 2006, ARAA, 44, 507

Woosley, S. E. and Heger, A. 2003, preprint (astro-ph/0309165)

β	$r_0 = 100$ km			
	\dot{r}/r , (a)	\dot{r}/r , (c)	$X_{^{56}\text{Ni}}$	X_{α}
0.2	105	2.3	0.612	0.314
0.8	32	6.1	0.488	0.449
1.4	4.8	14	0.327	0.590
2.0	0.62	28	0.189	0.667
2.6	0.07	32	0.131	0.635
β	$r_0 = 50$ km			
	\dot{r}/r , (a)	\dot{r}/r , (c)	$X_{^{56}\text{Ni}}$	X_{α}
0.2	120	3.1	0.582	0.355
0.8	52	9.6	0.422	0.523
1.4	5.2	27	0.229	0.689
2.0	0.62	58	0.079	0.752
2.6	0.06	64	0.048	0.705

Table 1: Average values of velocity divided by radial distance \dot{r}/r in units of s^{-1} for two sets of trajectories with entropy $s/k = 30$ and starting disk positions $r_0 = 100$ km and $r_0 = 50$ km from an AD-BH with $\dot{m} = 0.5$. Each set of trajectories includes five values of wind parameter β , and the average \dot{r}/r is calculated twice: (a) at early times as the electron fraction is set ($T_9 > 10$) and (c) at later times during nuclear reassembly ($6 > T_9 > 2$), where (a) and (c) correspond to the portions of the trajectory depicted in Fig. 2. Also included are the final mass fractions of ^{56}Ni and alpha particles for each trajectory.